

Study on Clamping Type DC Circuit Breaker with Short Fault Isolation Time and Low Energy Dissipation

Xibei Zhao, Gen Li, *Member, IEEE*, Jianzhong Xu, *Senior Member, IEEE*, and Jinsha Yuan

Abstract—The development of DC grids faces challenges from DC fault protection. The conventional DC circuit breaker (DCCB) employs metal-oxide varistor (MOV) to isolate the faulted line, in which the fault isolation process is coupled with the energy dissipation process. In this study, a clamping type DCCB (CTCB) using internal capacitors to clamp the converter voltage is proposed. Thanks to the proposed configuration, fault isolation and energy dissipation are decoupled, resulting in a fast fault isolation and low energy dissipation compared to the conventional DCCB. The working principle of the proposed CTCB is presented and verified in a DC grid simulation model. A comparison is made with the traditional DCCB. The fault isolation time can be reduced by 34.5%. The dissipated energy can be reduced by 17.4%. The energy dissipation power can be reduced by 76.2%.

Index Terms—DC circuit breaker, DC fault, DC protection, HVDC grid, MMC.

NOMENCLATURE

DCCB	Direct current circuit breaker.
LCS	Load commutation switch.
UFD	Ultra-fast disconnecter.
MB	Main breaker.
MOV	Metal-oxide varistor.
MVC	Main voltage clamper.
EAB	Energy absorption branch.
CLR	Current limiting reactor.
RCB	Residual current breaker.

I. INTRODUCTION

THE high voltage direct current (HVDC) grid based on the modular multilevel converter (MMC) is considered to be an effective solution for transferring renewable energy and AC grid interconnections [1]–[3]. The DC fault protection

is one of the most challenging obstacles that limits the wide application of DC grids. Therefore, significant attention has been paid to DC fault clearance methods from industry and academia [4], [5]. Due to the small circuit impedance of the DC grid, DC fault currents grow rapidly and the DC fault propagates very fast. Therefore, the fault current should be interrupted within a short period, e.g., 5 ms, to protect the converters from blocking.

A large fault current will also challenge the power rating of the energy dissipation devices, which are required to dissipate the residual energy within a few milliseconds to ensure a fast post-fault restoration. Thus, the applied energy dissipation devices may face risks under this high-power transient process. For instance, some modules may be damaged due to the unbalanced voltage-current sharing or overheating [6], [7]. Therefore, the DC grid fault clearing method must meet two basic requirements: 1) fast fault current isolation and 2) low energy dissipation.

A DC circuit breaker (DCCB) has been considered as one of the essential equipment to protect DC grids [8], [9], which can achieve a fully selective protection compared to methods based on converters with fault blocking capability [10], [11]. Although solid-state DCCBs can complete a fast fault current interruption, their high on-state losses are the main weakness that limits their applications. Hybrid DCCBs use the current commutation branch to realize a tradeoff between low conduction losses and fast interruption speed. ABB first proposed the concept of hybrid DCCB, which can interrupt 9 kA fault current in 3 ms. It uses a hybrid branch to conduct load current, and anti-series IGBTs are used to achieve bidirectional protection capability [8]. Alstom has developed its hybrid DCCB with 15 kA/3 ms fault interruption capability, in which thyristors are used to reduce the total cost [12], [13]. China State Grid has installed the first three engineering operating hybrid DCCBs with a capacity of 15 kA/3 ms in the Zhoushan 5-terminal 200 kV MMC-HVDC project [14], [15], in which full-bridge sub-modules are used to block the DC fault. In 2020, the 500 kV diode bridge-based hybrid DCCB with 25 kA capacity was operated in the Zhangbei DC grid [16].

Despite different topologies of the existing DCCBs, their core purpose is to force the fault current flow into the metal-oxide varistor (MOV). The MOV will insert a counter voltage into the fault circuit, and then the fault current will decrease by dissipating the fault energy [17], [18]. A large MOV resistance can quickly dissipate the fault energy. However, it needs a high

Manuscript received September 23, 2020; revised January 18, 2021; accepted February 3, 2021. Date of online publication November 13, 2021, date of current version May 31, 2022. This work was supported by National Key R&D Program 2018YFB0904600 and National Natural Science Foundation of China under grant 51777072.

X. B. Zhao (corresponding author, email: 1055248652@qq.com), J. Z. Xu, and J. S. Yuan are with the State Key Laboratory of Alternate Electrical Power System with Renewable Energy Sources, North China Electric Power University, Beijing 102206, China.

G. Li is with the Electric Energy Group, Department of Engineering Technology, Technical University of Denmark (DTU), 2750 Ballerup, Denmark.

DOI: 10.17775/CSEEJPES.2020.05180

energy dissipation power rating, which may result in a large dimension and high cost. An MOV with low resistance will reduce its requirement for a power rating, but will slow the fault isolation speed and enlarge the total dissipated energy. Moreover, the high-power rating or high energy dissipation of the MOV will both reduce its service life. In this case, it is of great significance to find an optimal solution which can balance the requirements of fault clearing speed and energy dissipation capacity.

In this study, a clamping type DCCB (CTCB) with a decoupled fault current decreasing and energy dissipation process is proposed. Capacitor modules are used to withstand the voltage differences between the DC bus and the faulted line. The faulted line can be isolated first, once the capacitor is fully charged at a zero current. The energy stored in the capacitor modules is then dissipated by its resistance-capacitor (RC) circuit rather than MOV. Moreover, a line-side bypass branch is also designed to help achieve the fast fault isolation and low energy dissipation.

The remainder of this paper is organized as follows. An introduction of the conventional hybrid DCCB is presented in Section II. The topology, working principle and parameter analysis of the proposed CTCB are presented in Section III. In Section IV, the performance of the proposed CTCB is verified in a four-terminal DC grid through simulations conducted in PSCAD/EMTDC. The comparisons of the proposed CTCB with the traditional DCCBs are provided in Section V. The conclusion is presented in Section VI.

II. PRINCIPLE OF THE TRADITIONAL HYBRID DCCB

The conventional hybrid DCCB is shown in Fig. 1, which is composed of a load commutation switch (LCS), an ultra-fast disconnecter (UFD), a main breaker (MB) and an MOV [8]. RCD snubber circuits are equipped for protecting the insulated-gate bipolar transistors (IGBTs). Moreover, a current limiting reactor (CLR) is used to limit the rate-of-rise of the fault current. A residual current breaker (RCB) is used to isolate the faulted line from the healthy circuit.

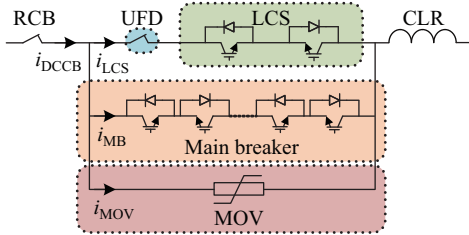


Fig. 1. Topology of the conventional hybrid DCCB.

The operation process of a DCCB can be divided into four stages: Before the fault is detected, the DC current flows through the LCS branch in stage I. Once a fault is detected, the MB is conducted, and the LCS will be immediately blocked. In stage II, the fault current commutates to the MB, and the UFD starts to open. The fault current will keep rising in stage II. From the beginning of stage III, the UFD is in open position, the MB is turned off to break the current. The fault current is

forced to the MOV branch and the fault energy is absorbed in the MOV. The fault current reaches zero at the end of stage III. Finally, the RCB is used to isolate the faulted line from the healthy grid in stage IV, see Fig. 2.

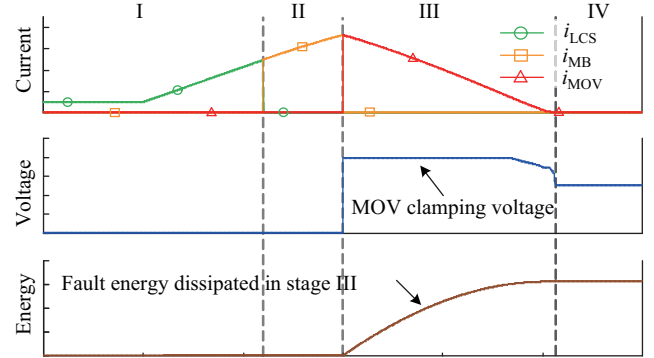


Fig. 2. Operation process of a DCCB.

As shown in Fig. 2, the fault current decreasing process and MOV energy dissipation is coupled in the conventional DCCB. The fault energy is all concentrated in the MOV in several milliseconds, which increases the burden of the MOVs, and limits a further reduction of the fault isolation speed. In this study, a new type of DCCB with decoupled fault isolation and energy dissipation is proposed, and the peak MOV power is also reduced by prolonging the energy dissipation process.

III. THE PROPOSED CLAMPING TYPE DCCB

A. Topology and Working Principle

The proposed CTCB is shown in Fig. 3. It consists of the UFD and LCS, the main voltage clammer (MVC) and the line-side energy absorption branch (EAB). It should be mentioned that the topology shown in Fig. 3 is unidirectional for the purpose of easy presenting. The bidirectional topology will be discussed in Section III-B.

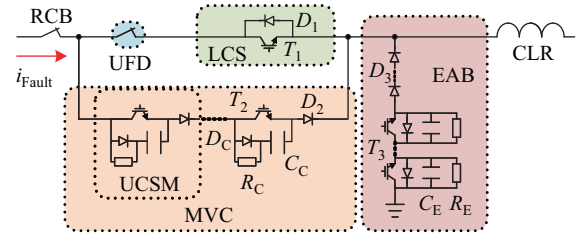


Fig. 3. Topology of the proposed CTCB.

The MVC consists of a number of series-connected unidirectional clamping sub-modules (UCSMs), which can force the fault current to charge the capacitors in one direction. The resistance R_C , diode D_C , and capacitor C_C form the RCD circuit which will dissipate the energy stored in C_C . The EAB provides a free-wheeling current path for the residual fault current in the faulted line. The diodes (D_3) in EAB are used to withstand the DC voltage in the normal state. C_E and R_E are employed to dissipate the fault energy stored in the CLR and fault current path once the IGBTs (T_3) are blocked.

Compared to the traditional DCCB, the proposed CTCB uses C_C to achieve DC fault isolation. The capacitor also acts as an energy storage station to absorb the fault energy. Then, the fault energy on the converter-side and line-side is separately dissipated, which can reduce the CB's overall requirements. However, the capacitor based DCCB [19], [20] only uses capacitors to assist the fault current transfer to the MOV, and the energy dissipation process is similar to the conventional DCCB.

There are four operational states of the proposed CTCB: normal operation, current commutation, voltage clamping and energy dissipation.

1) **Normal operation** ($t_0 \rightarrow t_1$): Assuming that the DC fault occurs at t_0 , and the fault will not be detected until t_1 . Only T_1 is conducted during the normal operation, the current flows through the LCS branch, as shown in Fig. 4(a).

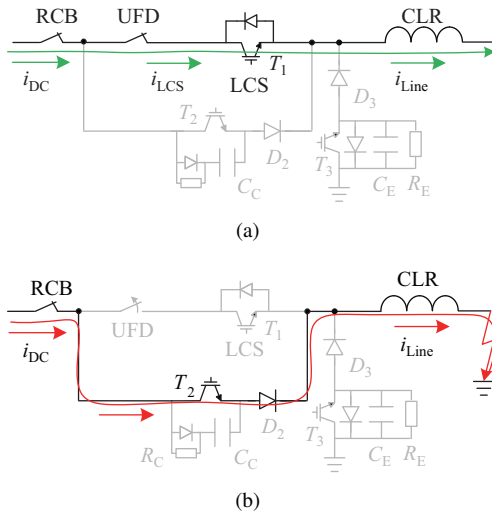


Fig. 4. Operational states of the proposed CTCB. (a) Normal operation $t_0 \rightarrow t_1$; (b) Current commutation $t_1 \rightarrow t_2$.

2) **Current commutation** ($t_1 \rightarrow t_2$): T_2 will be triggered and the LCS will be turned off once a DC fault is detected at t_1 . Then, as shown in Fig. 4(b), the current commutates to the MVC, and the UFD starts to open.

3) **Voltage clamping** ($t_2 \rightarrow t_4$): The UFD is fully opened at t_2 . Then, T_2 will be turned off to charge C_C . At the same time, T_3 is triggered to create a free-wheeling circuit to transfer the fault current, as shown in Fig. 5(a). There are two sub-states with the variation of the clamping capacitor voltage u_C .

① $u_C < u_S$ ($t_2 \rightarrow t_3$): u_C starts to rise from t_2 . The DC line voltage u_{Line} is equal to u_S minus u_C , thus it will keep decreasing. u_{Line} is also the voltage on the CLR, so the fault current will still keep rising, but the rate of rise will become slower with the u_{Line} decreasing. It should be mentioned that, during this period, there is no current in the free-wheeling circuit due to the line voltage u_{Line} still being over zero.

② $u_C = u_S$ ($t_3 \rightarrow t_4$): The line voltage u_{Line} will become zero when $u_C = u_S$ at t_3 . Then, the free-wheeling current i_E starts to flow through the EAB, as shown in Fig. 5(a). Because of the system inductance, the capacitor current i_C may not immediately decay to zero. Therefore, u_C will keep rising for

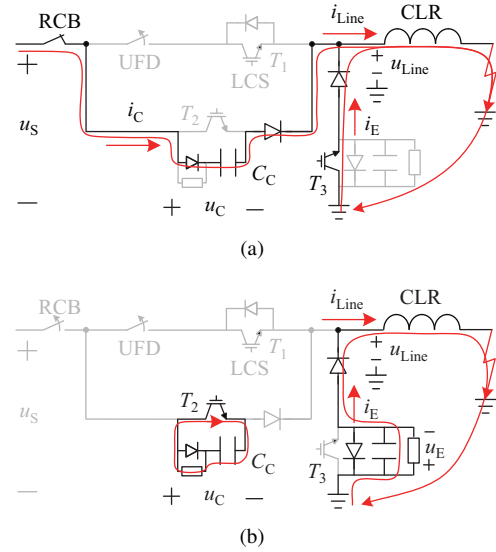


Fig. 5. Operational states of the proposed CTCB. (a) Voltage clamping state $t_2 \rightarrow t_4$; (b) Energy dissipation $t_4 \rightarrow t_6$.

a while. i_{Line} will totally transfer to the EAB once i_C becomes zero at t_4 .

4) **Energy dissipation** ($t_4 \rightarrow t_6$): The RCB starts to open at zero current after t_4 . The faulted line will be isolated from the healthy circuit once the RCB is fully opened at t_5 . Then, the fault energy is separately dissipated, as shown in Fig. 5(b). T_2 will be turned on to dissipate the energy stored in C_C until t_6 . T_3 is turned off to dissipate the residual energy stored in the CLR and DC line until t'_6 .

Based on the above analysis, the energy dissipation process is decoupled with the process of isolating the faulted line from the healthy circuit. The fault current from the healthy system is isolated first at t_4 , then the healthy circuit can start to recover from t_5 , leaving the CTCB to gradually dissipate the fault energy. This affords a long-time energy dissipation, which helps reduce the power rating of the RC circuit. Moreover, the electric process of the CTCB is also drawn in Fig. 6, in which shows that the fault current is isolated at t_4 , and then the fault energy is dissipated at t_6 .

B. Bidirectional CTCB and its Backup Protection

The backup protection capability is also a demand for the

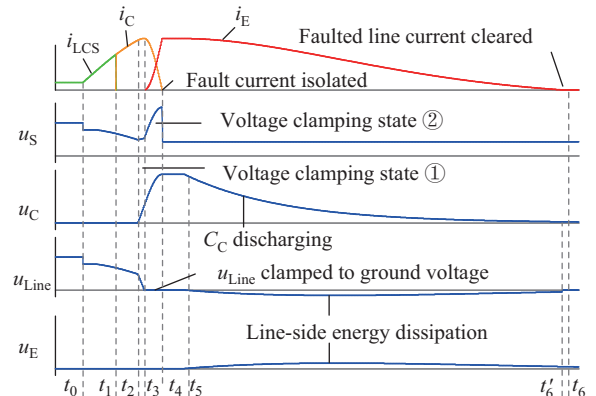


Fig. 6. Electric process of the proposed CTCB.

protection equipment. A portion of the DC grid is shown in Fig. A3, the fault current will always flow from the healthy system to the fault point in the DC grid. The DCCB is usually installed on the two ends of the over-head line, and the positive direction of CB_{12} is used for the primary protection of its transmission lines, see Fig. 7(a). The DCCB is usually designed as bidirectional equipment, and its backup protection is realized by the reverse direction of the adjacent CB_{13} , see Fig. 7(b). In some studies, unidirectional DCCBs are designed to reduce cost [21], [22]. Their backup protection can also be realized by the CB_{31} of the adjacent lines, but the speed and sensitivity of such a protection method are limited, see Fig. 7(c). As the near backup protection has more technical advantages, it is adopted by the existing projects.

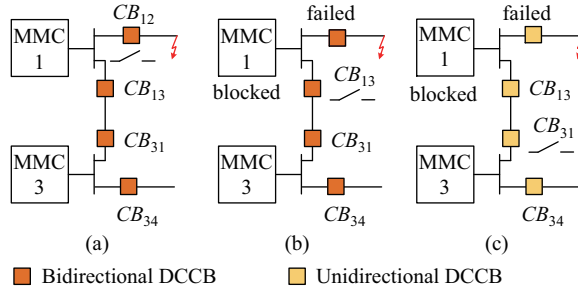


Fig. 7. Protection scheme. (a) Primary protection; (b) Bidirectional DCCB Backup protection; (c) Unidirectional DCCB Backup protection.

The CTCB can use the same backup protection method in Fig. 7(c), but a bidirectional topology will enhance its performance, see Fig. 8(a). A diode H-bridge is employed to cooperate with the MVC to achieve the bidirectional current breaking capability. Thanks to this configuration, only unidirectional clamping sub-modules are needed, which can reduce the use of power electronic devices. The EAB is unidirectional due to the direction of D_3 . However, the backup protection can still be realized by the proper coordination with other CTCBs, as illustrated in Fig. 8(b).

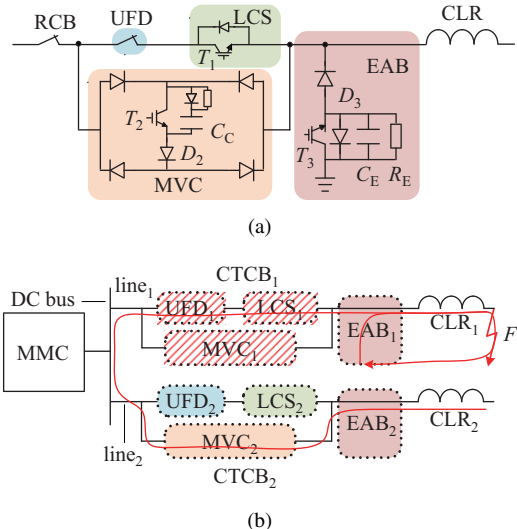


Fig. 8. Topology and back protection of the proposed CTCB. (a) Bidirectional CTCB; (b) Backup protection scheme.

Deployment of the proposed CTCBs at the terminal of an MMC with two DC lines is shown in Fig. 8(b). If $CTCB_1$ suffers a failure in case of a fault F_1 , $CTCB_2$ will be ready to protect the system. It should be mentioned that as EAB_2 can only provide a bypassing path for the faults in line₂, the proposed backup protection still needs the participation of EAB_1 . As illustrated in Fig. 8(b), the MVC_2 in $CTCB_2$ will coordinate with EAB_1 to achieve the backup protection. Considering that the EAB has a low failure rate due to the limited use of semiconductors, it is still reliable to ensure a secure backup protection. The CTCB only needs four additional diodes to achieve bidirectional protection, while DCCB often needs twice as many devices. Therefore, the investment of the bidirectional CTCB is lower.

In the primary and backup protection, the proposed CTCB can also use the main breaker instead of the main clamber. The fault clearing process will be similar, but the peak energy dissipation power is the same, and the fault isolation and energy dissipation is still coupled in the main breaker. However, the proposed CTCB will benefit from the reclosing process, but the main breaker cannot achieve a similar effect.

C. Reclosing Method of CTCB

After sufficient time for the fault line deionization, the CTCB can be reclosed by first closing the RCB. If the fault disappears, the DC line will be isolated by C_C . Then, the LCS and UFD are closed, and the system recovers to its initial state. If the fault still exists, a natural charging path is established, and the surge current will automatically charge C_C , see Fig. 9. Then the CTCB can repeat the process t_2-t_6 presented in Fig. 5 for a second-time breaking.

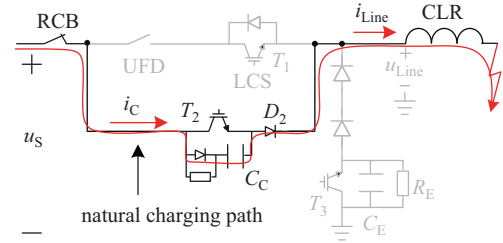


Fig. 9. Natural charging path of reclosing process.

Compared with traditional DCCB, the CTCB does not need any further action before the capacitor charging current disappears, thereby allowing enough time for fault detection. However, in the DCCB reclosing process, the protection detection must be quick enough to prevent the IGBT from overcurrent. The use of a capacitor ensures that T_2 does not need a second-time turn-off within a short time, enabling the IGBTs to avoid the reclosing surge current; thus, their service life is extended.

D. Mathematical Analysis of the Proposed CTCB

Figure 10 shows the equivalent circuit during the voltage clamping state, wherein the converter is represented as an RLC circuit [23].

As shown in Fig. 10, C_S , L_S and R_S are the equivalent circuit parameters of the converter. During t_2 to t_3 , the circuit

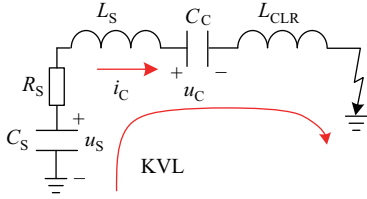


Fig. 10. Equivalent circuit of the voltage clamping state.

can be expressed as:

$$u_S - u_C - (L_S + L_{CLR}) \frac{di_C}{dt} - R_S i_C = 0, \quad (1)$$

$$-C_S \frac{du_S}{dt} = C_C \frac{du_C}{dt} = i_C. \quad (2)$$

The equation of i_C is obtained by substituting (2) into (1):

$$-(L_S + L_{CLR}) \frac{d^2 i_C}{dt^2} - R_S \frac{di_C}{dt} - \left(\frac{1}{C_S} + \frac{1}{C_C} \right) i_C = 0. \quad (3)$$

The expression of i_C is obtained by arranging (3):

$$i_C = C_{11} e^{\alpha_1 t} \cos(\beta_1 t) + C_{12} e^{\alpha_1 t} \sin(\beta_1 t). \quad (4)$$

The initial condition of Eq. (4) is:

$$i_C(t_{2+}) = i_C(t_{2-}), i'_C(t_{2+}) = \frac{u_S(t_{2-})}{L_S + L_{CLR}}. \quad (5)$$

Thus,

$$\begin{cases} C_{11} = i_C(t_{2-}), C_{12} = \frac{\frac{u_S(t_{2-})}{L_S + L_{CLR}} - C_{11} \alpha_1}{\beta} \\ \alpha_1 = -\frac{R_S}{2(L_S + L_{CLR})}, \beta_1 = \frac{\sqrt{4(L_S + L_{CLR}) \left(\frac{1}{C_S} + \frac{1}{C_C} \right) - R_S^2}}{2(L_S + L_{CLR})} \end{cases}. \quad (6)$$

The u_C can be written as:

$$u_C = \frac{\int_{t_2}^t i_C dt}{C_C} = \frac{1}{C_C(\alpha^2 + \beta^2)} [(C_{11}\alpha - C_{12}\beta)e^{\alpha_1 t} \cos \beta_1 t + (C_{12}\alpha + C_{11}\beta)e^{\alpha_1 t} \sin \beta_1 t - (C_{11}\alpha - C_{12}\beta)e^{\alpha_1 t_2} \cos \beta_1 t_2]. \quad (7)$$

The CTCB will change to the voltage clamping state ②, when u_C is equal to u_S . Then, the L_{CLR} will be bypassed from the circuit once the EAB is conducted, but other parts of the equations are similar. Therefore, state ② will not be studied further due to only the small differences that exist in the equations.

For the energy dissipation state, the discharging circuit of C_C in Fig. 5(b) is an RC circuit which has been well discussed in [24]. For the EAB, a single direction circuit can be obtained after turning off T_3 , as shown in Fig. 11.

Based on KVL and KCL, this process can be expressed as:

$$\begin{bmatrix} \frac{di_{Line}}{dt} \\ \frac{du_E}{dt} \end{bmatrix} = \begin{bmatrix} 0 & \frac{-1}{L_{CLR}} \\ \frac{1}{C_E} & \frac{-1}{R_E C_E} \end{bmatrix} \begin{bmatrix} i_{Line} \\ u_E \end{bmatrix}. \quad (8)$$

The equation of i_{Line} is obtained by arranging (7):

$$\frac{d^2 i_{Line}}{dt^2} + \frac{1}{C_E R_E} \frac{di_{Line}}{dt} - \frac{i_{Line}}{L_{CLR} C_E} = 0. \quad (9)$$

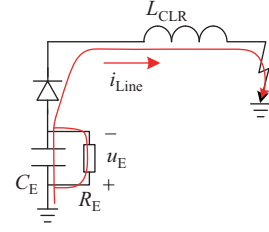


Fig. 11. Equivalent circuit of the energy absorption state.

The expression of i_{Line} is obtained:

$$i_{Line} = C_{21} e^{\alpha_2 t} \cos(\beta_2 t) + C_{22} e^{\alpha_2 t} \sin(\beta_2 t). \quad (10)$$

The initial condition of Eq. (10) is:

$$i_{Line}(t_{5+}) = i_{Line}(t_{5-}), i'_{Line}(t_{5+}) = 0, \quad (11)$$

where

$$\begin{cases} C_{21} = i_{Line}(t_{5-}), C_{22} = -\frac{C_{21} \alpha_2}{\beta_2} \\ \alpha_2 = \frac{-1}{2R_E C_E}, \beta_2 = \frac{\sqrt{\frac{4}{L_{CLR} C_E} - \left(\frac{1}{R_E C_E} \right)^2}}{2} \end{cases}. \quad (12)$$

The u_E can be written as:

$$u_E = C_{31} e^{\alpha_3 t} \cos(\beta_3 t) + C_{32} e^{\alpha_3 t} \sin(\beta_3 t). \quad (13)$$

The initial condition of Eq. (13) is:

$$u_E(t_{5+}) = 0, u'_E(t_{5+}) = \frac{i_{Line}(t_{5-})}{\beta_3}, \quad (14)$$

where

$$\begin{cases} C_1 = 0, C_2 = \frac{i_{dc}(0)}{\beta} \\ \alpha = \frac{-1}{2R_B C_B}, \beta = \frac{\sqrt{\left(\frac{1}{R_B C_B} \right)^2 + \frac{4}{L_B C_B}}}{2} \end{cases}. \quad (15)$$

The mathematical analysis can help with understanding the inner principle of the proposed CTCB. The correctness of the math equations is verified in the MATLAB, but not shown in the paper due to over length.

IV. CASE STUDY

A. Test System

The performance of the CTCB is verified in the Zhangbei four-terminal bipolar DC grid [16], as shown in Fig. 12. The converter control modes and system parameters are listed in the Appendix. All models are built in PSCAD/EMTDC V4.6 with a simulation time step of 10 μ s.

A pole-to-pole fault f_1 is used to demonstrate the protection process of the proposed CTCB. Moreover, a high resistance pole-to-ground fault f_2 is used to verify CTCB's performance under high impedance faults. The fault resistance R_f is set as 100 Ω and 200 Ω . Both f_1 and f_2 are initiated at $t = 1$ s. The measurements of u_S , i_{DC} and i_{Line} are shown in Fig. 12. Other measurements of the CTCB are shown in Figs. 4 and 5. The CTCB needs numerous components in series to withstand the fault voltage, but the equivalent values of C_C , R_C , C_E , R_E are set as 30 μ F, 250 Ω , 1000 μ F, and 10 Ω , respectively. The used 30 μ F capacitor equals the equivalent capacitance of one arm in station 1 (250 cascade HBSMs with 7500 μ F

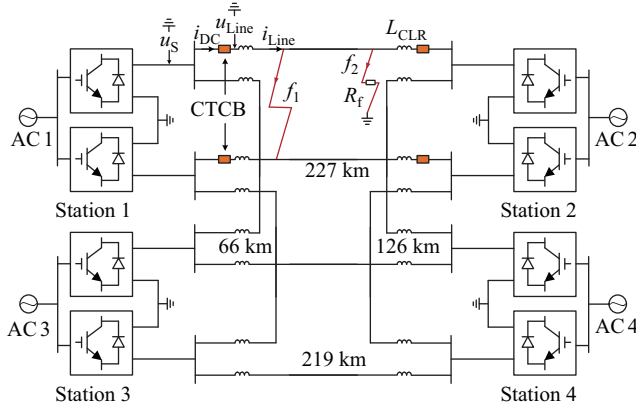


Fig. 12. Topology of four-terminal DC grid.

capacitor), so it is realistic in the project. The fault detection time is set as 3 ms after the fault wave arrives the CTCB, and the operation time of UFD is 2 ms. Thus, C_C will not be charged within the initial 5 ms after the fault.

B. Pole-to-pole Large Current Interruption

The performance of interrupting large currents of the CTCB is verified by the pole-to-pole fault f_1 . Currents and voltages of the CTCB are shown in Figs. 13 (a) and (b). Fig. 13(c) shows the operating status of CTCB's components, wherein the high and low levels mean that the switch is ON and OFF. The definition of the time sequences is the same as Section III-A.

In Fig. 13, the fault occurs at $t_0 = 1$ s and is detected at $t_1 = 1.003$ s. T_1 is turned off at t_1 and the fault current commutates to the MVC. At $t_2 = 1.005$ s, IGBT T_2 is turned off, then the fault current starts to charge C_C . u_C rises from zero voltage and the fault current keeps rising during t_2 - t_3 .

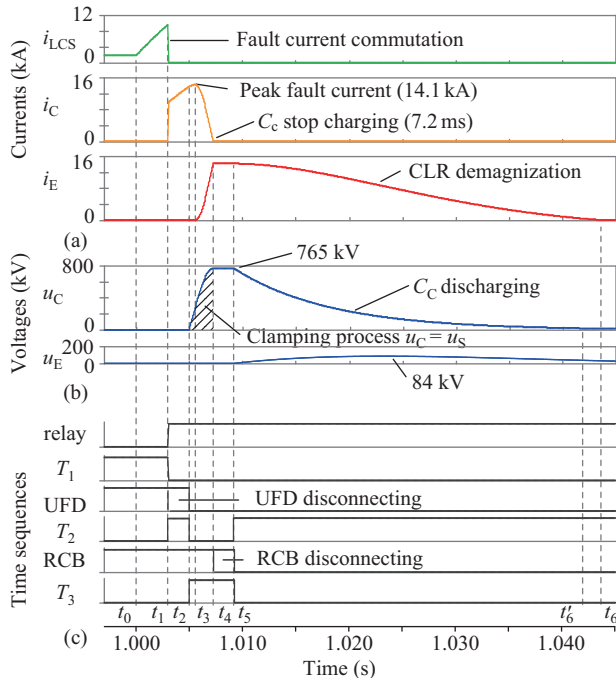


Fig. 13. Operating process of CTCB under large current. (a) Currents; (b) Voltages; (c) Time sequences.

At $t_3 = 1.0053$ s, u_C is equal to u_S and i_C starts to decrease. EAB provides a free-wheeling path for the current in CLR, so i_E increases while i_C decreases. At $t_4 = 1.0072$ s, i_C reaches zero and RCB operates to isolate the faulted line. At $t_5 = 1.0092$ s, RCB opens successfully. Then, T_2 is triggered and T_3 is turned off and the energy stored in C_C and CLR starts to be dissipated by R_C and R_E . At last, the whole process ends at $t_6 = 1.0434$ s when i_E becomes zero.

The currents and voltages of the DC grid are shown in Fig. 14. It can be seen that the isolation of the faulted line is decoupled with the decay of the residual fault current. As isolating the faulted circuit is the top priority of protection for the DC grid, the proposed CTCB provides the solution for achieving a fast fault isolation. The following energy dissipation process helps reduce the power rating of R_C and R_E . During t_3 - t_4 , the DC bus voltage u_S follows the change of u_C , which is clamped by C_C , instead of collapsing a lot after the fault. This will be beneficial to the post-fault restoration. The healthy system starts to recover after the clamping process. Although the DC line current i_{Line} continues decaying until t_6 , the faulted line has already been isolated from the DC system and therefore, it won't affect the healthy circuits. The line-side elements all have high surge capability, so a long tail energy dissipation process is acceptable.

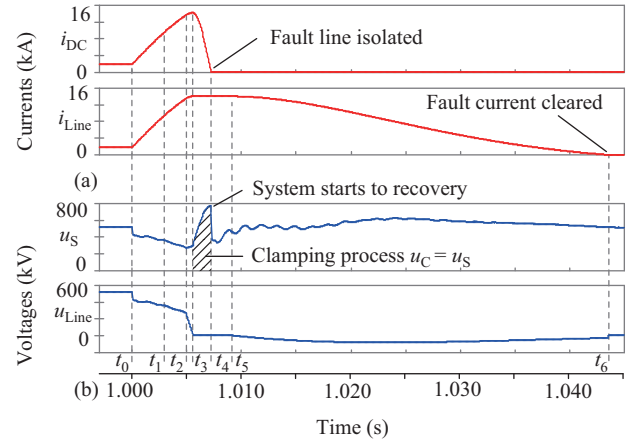


Fig. 14. System dynamics (a) Currents; (b) Voltages.

Based on the above results, the following features of the proposed CTCB are determined: 1) The DC voltage is clamped by the internal capacitor of the CTCB, which helps the post-fault restoration; 2) The isolation of the faulted line and its energy dissipation are decoupled, which achieves a fast isolation and low energy dissipation. 3) There are no sudden changes of fault current and IGBT voltages, which can mitigate the transient rate-of-change of the IGBT's voltage and therefore, reduce their manufacturing difficulty. These advantages will be future discussed in Section V.

C. Pole-to-ground Small Current Interruption

A pole-to-ground fault f_2 with different fault resistance R_f (100 and 200 Ω) was tested. Fig. 15 shows the simulation results under $R_f = 100 \Omega$. The fault current increases slowly with large fault resistance, and the fault resistance can also

help dissipate the line-side energy. The fault is detected 3 ms after the transmission wave reaches the relay, at $t_1 = 1.0037$ s. C_C starts to be charged at $t_2 = 1.0057$ s. However, due to the small current, the voltage clamping process of charging C_C is long. The faulted line is isolated until $t_4 = 1.0124$ s. Then, the residual fault energy is dissipated by both R_E and R_f from $t_5 = 1.0145$ s to $t_6 = 1.0437$ s. The CTCB needs 12.4 ms to isolate the faulted line. This can be acceptable, considering that the small fault current may cause less damage to the system. As shown in Fig. 15(b), the peak voltages of u_C and u_E are also reduced under the high resistance fault.

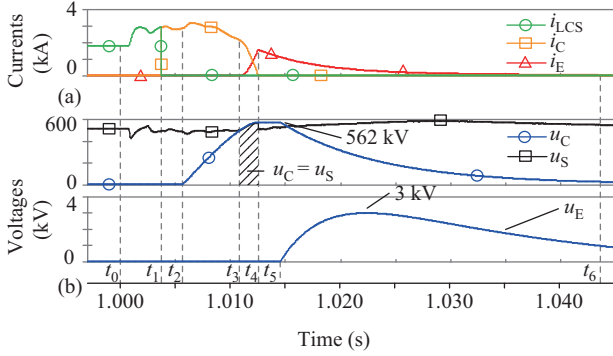


Fig. 15. CTCB performance under $R_f = 100 \Omega$. (a) Currents; (b) Voltages.

The CTCB has a different performance under a higher fault resistance, e.g., $R_f = 200 \Omega$. Fault current rises less than the last case, as shown in Fig. 16. The high fault resistance results in less voltage drop of u_S . Therefore, the voltage clamping process is longer compared to the last case until $t_3 = 1.027$ s. The fault energy is primarily dissipated by fault resistance. Therefore, the magnitudes of i_E and u_E are low. Although the fault clearing process needs a long time under a high resistance fault, it still can be acceptable. This scenario has less challenge to the system than a large current fault, thus the system can afford more time for the fault clearing.

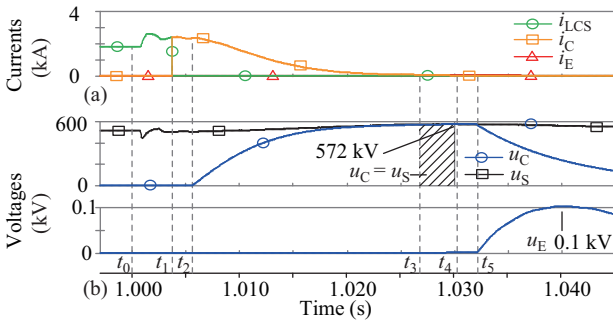


Fig. 16. CTCB performance under $R_f = 200 \Omega$. (a) Currents; (b) Voltages.

V. ENERGY STORAGE AND DISSIPATION ANALYSIS

A. Capacitor Storage Demand Analysis

As a core component of the proposed CTCB, the C_C and C_E have significant influences on the performance of the CTCB. A smaller capacitance of C_C can be charged faster, which will benefit in a quick fault isolation and system recovery. However,

a small capacitor may need to face a higher overvoltage. Considering the difficulty of manufacture, the capacitance of C_C is chosen as $30 \mu\text{F}$. the same value as the equivalent capacitance within one upper or lower arm in the Zhangbei project (250 cascade HBSMs with $7500 \mu\text{F}$ capacitor), which is practical for industrial realization.

The EAB also affects the voltage clamping process. A large capacitor will be needed if there is no EAB [25]. In the following studies, i_{DC} and u_C under four different cases are compared to show the influence from the capacitors and EAB: 1) small capacitor ($30 \mu\text{F}$) with EAB; 2) small capacitor without EAB 3) large capacitor ($100 \mu\text{F}$) with EAB and 4) large capacitor without EAB, as shown in Fig. 17.

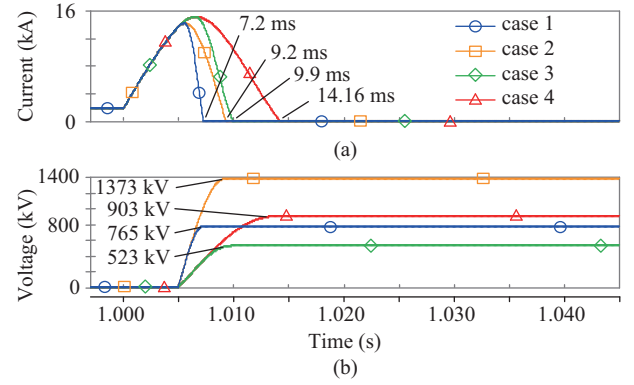


Fig. 17. Comparisons of i_{DC} and u_C under four different cases. (a) Currents; (b) Voltages.

It can be seen from Fig. 17 that a small capacitor can achieve a fast fault isolation. Comparing Cases 1 and 3, 2.7 ms can be reduced by the small capacitor. $u_C = 765$ kV in Case 1 is higher than $u_C = 523$ kV in Case 2. However, both cases can be acceptable if the converter can continue operating under 810 kV [16]. Comparing Cases 1 and 2, 2 ms can be reduced for the isolation thanks to the deployment of the EAB. Both Cases 2 and 4 need a large C_C which may be impractical for real applications and the fault isolation time is too long.

The above analysis shows that Case 1 with a small capacitor and EAB has the fastest fault isolation time and the second highest capacitor voltage. However, the capitol cost of the capacitor is significant, considering its capacity, as shown in Table I. Case 1 is preferred due to the fact it has the lowest energy storage requirement among the four cases, so the proposed scheme of CTCB is able to achieve a fast isolation and lower requirements for the internal capacitor.

TABLE I
COMPARISONS OF C_C

Items	Equivalent capacitance	Voltage	Total energy
Case 1	$30 \mu\text{F}$	765 kV	8.77 MJ
Case 2	$30 \mu\text{F}$	1373 kV	28.27 MJ
Case 3	$100 \mu\text{F}$	523 kV	13.67 MJ
Case 4	$100 \mu\text{F}$	903 kV	40.77 MJ

B. Comparison with the Conventional Hybrid DCCB

As a well-known HVDC switchgear, the hybrid DCCB proposed by ABB is selected to compare with the CTCB in

terms of: 1) electrical processes during the fault protection; 2) rate-of-change of IGBT's voltage; 3) total dissipation energy and its power rating.

The studied DCCBs are the same as shown in Section II, the total clamping voltage of DCCB is 800 kV. The DC fault is detected at $t = 1.003$ s. The operation delay of the UFD is set as 2 ms. Therefore, the MOV will be inserted at 1.005 s, which is the same as the C_C of CTCB.

Figure 18 shows the currents and voltages of the proposed CTCB and ABB's DCCB under the same fault f_1 . It can be seen that the peak fault current of the CTCB is slightly higher than that of ABB's DCCB. This is because the C_C within CTCB needs a charging process before the decrease of the fault current. The fault current i_{DC} of CTCB decreases to zero at $t = 1.0072$ s, which is 3.8 ms (34.5%) faster than ABB's DCCB whose fault current i_{DCCB} decreases to zero at $t = 1.011$ s. Therefore, the proposed CTCB can isolate the faulted line from the healthy circuit faster than ABB's DCCB.

The dissipated energy and power are shown in Fig. 19. In Fig. 19(a), the dissipated energy of the MOV of ABB's DCCB is $E_{MOV} = 28.7$ MJ. The dissipated energy by CTCB's C_C

and C_E is 8.8 MJ and 3.5 MJ. Fig. 19(b) shows the energy stored in the CLR. The peak energy of E_{CLR_DCCB} is 14.5 MJ, but the total energy dissipation in the MOV is 28.7 MJ due to the coupled fault isolation and energy dissipation. The peak energy of E_{CLR_CTCB} is 14.9 MJ. Therefore, the dissipated energy in the CTCB is 23.7 MJ (8.8+14.9 MJ) which is 17.4% lower than ABB's DCCB. ABB's DCCB needs to dissipate bulk power in several milliseconds. In this case, its peak power is 11000 MW, while the CTCB has much lower peak power of 2610 MW (1900+710 MW), as shown in Fig. 19(c).

Thanks to the decoupled fault isolation and energy dissipation processes, the CTCB can significantly reduce the total dissipation energy and power, which is helpful to reduce the volume of equipment. As shown in Table II, the total dissipation energy, the peak and average power of CTCB has been reduced by 17.4%, 76.2%, and 87.6% compared to its ABB counterpart. Less fault energy indicates the system suffers less disturbance during the fault, and a lower power will reduce the volume for the resistors.

TABLE II
COMPARISONS OF ENERGY AND POWER DISSIPATION

Items	DCCB	CTCB	Reduced by
Total energy	28.7 MJ	23.7 MJ	17.4%
Peak power	11000 MW	2610 MW	76.2%
Average power	4783 MW	592 MW	87.6%

C. Semiconductors Requirements Comparison

The comparison of the energy storage element has been given in Section V.B, the requirements for semiconductors are given in this sub-section.

Assuming that all used semiconductors are 4.5 kV devices in a 500 kV DC grid, and redundant devices are not considered, CTCB and DCCB's semiconductor requirements are shown in Table III. The DCCB's main breaker needs 178 series-connected IGBTs and diodes in one direction. The CTCB needs 170 IGBTs and 340 diodes in series for its MVC, and 19 IGBTs and 112 diodes in series for its EAB. Further considering the bidirectional design, the semiconductor requirements for DCCB are doubled, but the CTCB only needs four more diodes. Therefore, the use of high price IGBTs is reduced in CTCB.

TABLE III
SEMI-CONDUCTOR COST CALCULATION

Items	ABB DCCB	CTCB
IGBTs	356	189
diodes	356	456
Total cost (p.u.)	391.6	234.6

At the same voltage level, diodes are much cheaper than IGBTs [24]. Suppose the cost of diodes is 10% of IGBTs, the per-unit cost of DCCB and CTCB are also given in Table III. It shows that by using fewer IGBTs, the total cost is reduced by around 40% compared to ABB's DCCB, making CTCB a promising solution for future DC protection equipment.

VI. CONCLUSIONS

This paper proposes a clamping type DCCB (CTCB) with

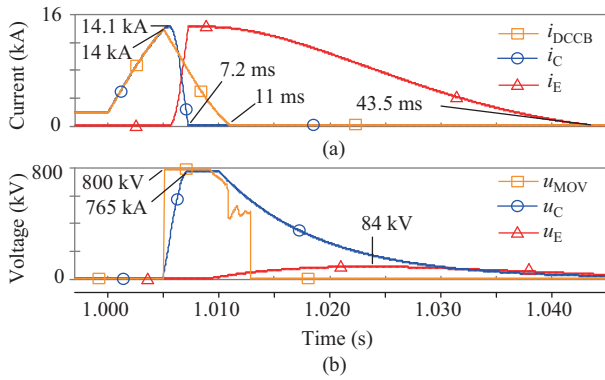


Fig. 18. Electrical processes of CTCB and ABB's DCCB. (a) Currents; (b) Voltages.

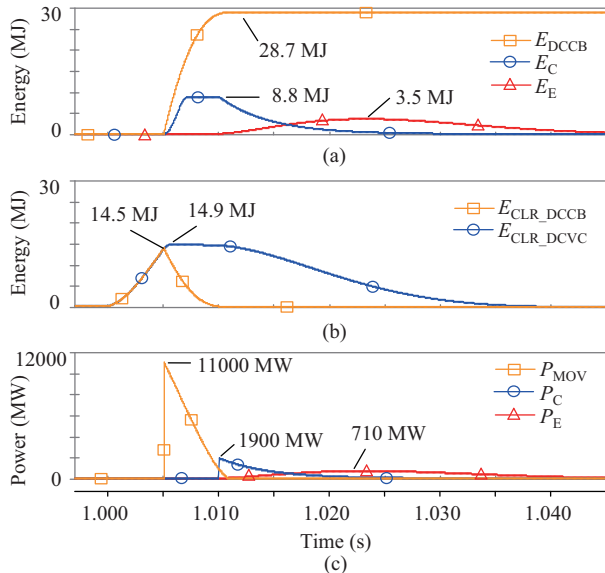


Fig. 19. Energy and power dissipation of CTCB and ABB's DCCB. (a) Dissipated energy. (b) CLR energy. (c) Energy dissipation power.

short fault isolation time and low energy dissipation. The proposed CTCB utilizes a branch of capacitors to isolate the DC current, and achieves fast isolation of the faulted line. An energy absorption branch is used to provide a free-wheeling current path to achieve low energy dissipation. Thanks to the proposed configuration, the processes of the fault isolation and energy dissipation are decoupled. Therefore, a fast post-fault restoration can be realized by quickly restarting the safely protected converter station. The primary protection, backup protection and reclosing logic of CTCB is discussed, and its performance is verified in the DC grid simulation.

In this study, the proposed CTCB can isolate the faulted line within 7.2 ms, or 34.5% less than ABB's DCCB. The energy dissipation of IGBTs and its peak power is also reduced by 17.4% and 76.2%, respectively. By comparing the requirements for semiconductors, the proposed CTCB can save 40% cost on IGBTs and diodes, making the proposed CTCB a potential solution for DC protection.

The proposed CTCB still has some potential drawbacks. The EAB needs to withstand DC rating voltage under normal state, but the long-term insulation ability of series-connected diodes still needs more consideration. Moreover, if EAB fails, the near backup protection cannot be achieved. Therefore, the performance of the EAB may affect the protection performance of CTCB.

APPENDIX

The DC grid model is based on the Zhangbei project [16]. Parameters of the four stations are given in Table AI. The control modes of the DC grid are given in Table AII.

TABLE AI
PARAMETERS OF THE MMCS

Items	MMCs 1&2	MMCs 3&4
AC voltage	230 kV	500 kV
Transformer Capacity	1700 MW	3400 MW
Transformer Leakage	0.1 pu	0.15 pu
Arm Inductance	0.06 H	0.1 H
SM Number	250	250
SM Capacity	7500 μ F	15000 μ F
CLR Inductance	150 mH	150 mH

TABLE AII
CONTROL MODES OF THE DC GRID

Station 1	active power	$P_N = 1500$ MW
	reactive power	$Q_N = 150$ Mvar
Station 2	active power	$P_N = 1500$ MW
	reactive power	$Q_N = 150$ Mvar
Station 3	active power	$P_N = 3000$ MW
	reactive power	$Q_N = 300$ Mvar
Station 4	DC voltage	$U_{DC} = \pm 500$ kV
	reactive power	$Q_N = 300$ Mvar

REFERENCES

- [1] T. An, X. X. Zhou, C. D. Han, Y. N. Wu, Z. Y. He, H. Pang, and G. Tang, "A DC grid benchmark model for studies of interconnection of power systems," *CSEE Journal of Power and Energy Systems*, vol. 1, no. 4, pp. 101–109, Dec. 2015.
- [2] X. B. Zhao, L. X. Chen, G. Li, J. Z. Xu, and J. S. Yuan, "Coordination method for DC fault current suppression and clearance in DC grids," *CSEE Journal of Power and Energy Systems*, to be published.
- [3] J. M. Carrasco, L. G. Franquelo, J. T. Bialasiewicz, E. Galvan, R. C. Portilloiguisado, M. A. M. Prats, J. I. Leon, and N. Moreno-Alfonso, "Power-electronic systems for the grid integration of renewable energy sources: a survey," *IEEE Transactions on Industrial Electronics*, vol. 53, no. 4, pp. 1002–1016, Jun. 2006.
- [4] J. Yang, J. E. Fletcher, and J. O'Reilly, "Short-circuit and ground fault analyses and location in VSC-based DC network cables," *IEEE Transactions on Industrial Electronics*, vol. 59, no. 10, pp. 3827–3837, Oct. 2012.
- [5] X. Han, W. X. Sima, M. Yang, L. C. Li, T. Yuan, and Y. Si, "Transient characteristics under ground and short-circuit faults in a ± 500 kV MMC-based HVDC system with hybrid DC circuit breakers," *IEEE Transactions on Power Delivery*, vol. 33, no. 3, pp. 1378–1387, Jun. 2018.
- [6] N. Tsukamoto, S. Imato, Y. Baba, and M. Ishii, "Current distribution in MOV element stressed by 4/10 μ s impulse current," in *2016 33rd International Conference on Lightning Protection (ICLP)*, Estoril, 2016, pp. 1–4.
- [7] J. Magnusson, R. Saers, L. Liljestrand, and G. Engdahl, "Separation of the energy absorption and overvoltage protection in solid-state breakers by the use of parallel varistors," *IEEE Transactions on Power Electronics*, vol. 29, no. 6, pp. 2715–2722, Jun. 2014.
- [8] A. Hassanpoor, J. Häfner, and B. Jacobson, "Technical assessment of load commutation switch in hybrid HVDC breaker," *IEEE Transactions on Power Electronics*, vol. 30, no. 10, pp. 5393–5400, Oct. 2015.
- [9] Y. X. Guo, G. Wang, D. H. Zeng, H. F. Li, and C. Hong, "A thyristor full-bridge-based DC circuit breaker," *IEEE Transactions on Power Electronics*, vol. 35, no. 1, pp. 1111–1123, Jan. 2020.
- [10] B. Li, J. W. He, Y. Li, and R. S. Li, "A novel solid-state circuit breaker with self-adapt fault current limiting capability for LVDC distribution network," *IEEE Transactions on Power Electronics*, vol. 34, no. 4, pp. 3516–3529, Apr. 2019.
- [11] K. Sano and M. Takasaki, "A surgeless solid-state DC circuit breaker for voltage-source-converter-based HVDC systems," *IEEE Transactions on Industry Applications*, vol. 50, no. 4, pp. 2690–2699, Jul.-Aug. 2014.
- [12] W. Grieshaber and L. Violleau, "Development and test of a 120 kV direct current circuit breaker," in *Proceedings of CIGRE Session*, Paris, France, 2014, pp. B4–301.
- [13] A. J. Far and D. Jovicic, "Design, modeling and control of hybrid DC circuit breaker based on fast thyristors," *IEEE Transactions on Power Delivery*, vol. 33, no. 2, pp. 919–927, Apr. 2018.
- [14] G. F. Tang, Z. Y. He, H. Pang, X. M. Huang, and X. P. Zhang, "Basic topology and key devices of the five-terminal DC grid," in *CSEE Journal of Power and Energy Systems*, vol. 1, no. 2, pp. 22–35, Jun. 2015.
- [15] W. D. Zhou, X. G. Wei, S. Zhang, G. F. Tang, Z. Y. He, J. C. Zheng, Y. H. Dan, and C. Gao, "Development and test of a 200kV full-bridge based hybrid HVDC breaker," in *2015 17th European Conference on Power Electronics and Applications (EPE'15 ECCE-Europe)*, Geneva, 2015, pp. 1–7.
- [16] H. Pang and X. G. Wei, "Research on key technology and equipment for Zhangbei 500kV DC grid," in *2018 International Power Electronics Conference (IPEC-Niigata 2018 -ECCE Asia)*, Niigata, 2018, pp. 2343–2351.
- [17] D. Jovicic, G. F. Tang, and H. Pang, "Adopting circuit breakers for high-voltage dc networks: appropriating the vast advantages of dc transmission grids," *IEEE Power and Energy Magazine*, vol. 17, no. 3, pp. 82–93, May-Jun. 2019.
- [18] A. Shukla and G. D. Demetriades, "A survey on hybrid circuit-breaker topologies," *IEEE Transactions on Power Delivery*, vol. 30, no. 2, pp. 627–641, Apr. 2015.
- [19] M. Zhou, W. Xiang, W. P. Zuo, W. X. Lin, and J. Y. Wen, "A novel HVDC circuit breaker for HVDC application," *International Journal of Electrical Power & Energy Systems*, vol. 109, pp. 685–695, Jul. 2019.
- [20] D. Jovicic, "Fast commutation of DC current into a capacitor using moving contacts," *IEEE Transactions on Power Delivery*, vol. 35, no. 2, pp. 639–646, Apr. 2020.
- [21] G. Chaffey and T. C. Green, "Directional current breaking capacity requirements for HVDC circuit breakers," in *2015 IEEE Energy Conversion Congress and Exposition (ECCE)*, Montreal, 2015, pp. 5371–5377.
- [22] C. Y. Li, J. Liang, and S. Wang, "Interlink hybrid DC circuit breaker," *IEEE Transactions on Industrial Electronics*, vol. 65, no. 11, pp. 8677–8686, Nov. 2018.
- [23] C. Y. Li, C. Y. Zhao, J. X. Xu, Y. K. Ji, F. Zhang, and T. An, "A pole-to-pole short-circuit fault current calculation method for DC grids," *IEEE*

Transactions on Power Systems, vol. 32, no. 6, pp. 4943–4953, Nov. 2017.

- [24] Q. Song, R. Zeng, Z. Q. Yu, W. H. Liu, Y. L. Huang, W. B. Yang, and X. Q. Li, "A modular multilevel converter integrated with DC circuit breaker," *IEEE Transactions on Power Delivery*, vol. 33, no. 5, pp. 2502–2512, Oct. 2018.
- [25] Z. Xu, H. Q. Xiao, and Y. Z. Xu, "Two basic ways to Realise DC circuit breakers," *The Journal of Engineering*, vol. 2019, no. 16, pp. 3098–3105, Mar. 2019.



and protection.

Xibei Zhao received the B.S degree in Electrical Engineering and Its Automation from Chongqing University (CQU) in 2015, and Ph.D. degree in Electrical Engineering in North China Electric Power University (NCEPU) in 2021. From Aug. 2019 to Oct. 2020, he was a joint Ph.D. student at Cardiff University. From Apr. 2021 to Jul. 2022, he was an energy planning engineer at China Electric Power Planning and Engineering Institute (EPPEI). Currently he is a lector at NCEPU since Aug. 2022. His research interests include HVDC grid operation



tromagnetic transient modeling, control, and protection of MMC-HVDC and DC grid.

Jianzhong Xu (M'14) received a B.S. in Thermal Power and Its Automation and a Ph.D. degree in Electrical Engineering from North China Electric Power University (NCEPU), Beijing, China, in 2009 and 2014, respectively. From 2012 to 2013 and 2016 to 2017, he was a joint Ph.D. student and Postdoctoral Fellow with the University of Manitoba. He is currently an Associate Professor with the State Key Laboratory of Alternate Electrical Power System with Renewable Energy Sources, NCEPU.

His research interests include the high-speed elec-



Jinsha Yuan received an M.E. degree in Theoretical Electrical Engineering and a Ph.D. degree in Electrical Engineering and Its Automation from North China Electric Power University, Baoding, China, in 1987 and 1992, respectively. He is currently a Professor and a Ph.D. Supervisor with North China Electric Power University, Baoding. His research interests include intelligent information processing technology, wireless communication, and electromagnetic field numerical calculation method and application.



Gen Li (M'18–SM'23) received the B.Eng. degree in Electrical Engineering from Northeast Electric Power University, Jilin, China, in 2011, the M.Sc. degree in Power Engineering from Nanyang Technological University, Singapore, in 2013 and the Ph.D. degree in Electrical Engineering from Cardiff University, Cardiff, U.K., in 2018. He is now an Associate Professor in Power System at the Technical University of Denmark (DTU), Denmark. From 2013 to 2016, he has been a Marie Curie Early Stage Research Fellow funded by the European

Commission's MEDOW project. He has been a Visiting Researcher at China Electric Power Research Institute and Global Energy Interconnection Research Institute, Beijing, China, at Elia, Brussels, Belgium and at Toshiba International (Europe), London, U.K. He was a Research Associate at the School of Engineering, Cardiff University from 2018 to 2022. His research interests include control and protection of HV and MV DC technologies, offshore wind, offshore energy islands, reliability modelling and evaluation of power electronics systems. Dr. Li is a Chartered Engineer in the U.K., a Young Editorial Board Member of *Applied Energy*, an Associate Editor of the *CSEE Journal of Power and Energy Systems*, an Editorial Board Member of *CIGRE ELECTRA* and *Global Energy Interconnection* and an IET Professional Registration Advisor. His Ph.D. thesis received the First CIGRE Thesis Award in 2018. He is now a Committee Member of IEEE PES Denmark.